Faraday Discussions

Cite this: DOI: 10.1039/c8fd00210j

PAPER

Ultrafast transient absorption spectroscopy of doped P3HT films: distinguishing free and trapped polarons

Matthew G. Voss, D. Tyler Scholes, J. Reddy Challa and Benjamin J. Schwartz *

Received 27th November 2018, Accepted 14th December 2018
DOI: 10.1039/c8fd00210j

It is generally presumed that the vast majority of carriers created by chemical doping of semiconducting polymer films are coulombically trapped by the counteranion, with only a small fraction that are free and responsible for the increased conductivity essential for organic electronic applications. At higher doping levels, it is also possible for bipolarons to form, which are expected to be less conductive than single polarons. Unfortunately, there is no simple way to distinguish free polarons, trapped polarons and bipolarons using steady-state spectroscopy. Thus, in this work, we use ultrafast transient absorption spectroscopy to study the dynamics of polarons in 2,3,5,6-tetrafluoro-7,7,8,8-tetracyanoquinodimethane (F4TNCQ)-doped films of poly(3-hexylthiophene-2,5-diyl) (P3HT) as a function of dopant concentration and excitation wavelength. When exciting on the red side of the polaron P1 transition, our transient absorption spectra and kinetics match well with what is expected for free 2-D-delocalized polarons; the measurements are not consistent with a recent theory of doped conjugated polymer electronic structure that suggests that the half-filled state lies deeper in the conduction band rather than in the bandgap. As we tune the excitation wavelength to the blue, our measurements reveal an increasing amount of slower transient kinetics that are consistent with the presence of coulombically-trapped polarons rather than bipolarons. Taking advantage of their distinct ultrafast relaxation kinetics as a type of action spectroscopy, we are able to extract the steady-state absorption spectra of free and trapped polarons as a function of dopant concentration. By comparing the results to theoretical models, we determine that in F4TCNQ-doped P3HT films, trapped polarons sit ~0.4 nm away from the anion while free polarons reside between 0.7 and 0.9 nm from the counteranion. Perhaps counterintuitively, the ratio of trapped to free polarons increases at higher doping levels, an observation that is consistent with a plateau in the concentration-dependent conductivity of F4TCNQ-doped P3HT films.

Department of Chemistry and Biochemistry, University of California Los Angeles (UCLA), Los Angeles, CA 90095-1569, USA. E-mail: schwartz@chem.ucla.edu

1 Introduction

Like all organic semiconductors, conjugated polymers have several disadvantages relative to their inorganic counterparts when it comes to serving as functional electronic materials. The conductivity of conjugated polymers is generally poor, the result of intrinsically low charge mobilities and meager equilibrium carrier densities. As with inorganic materials, the carrier density and mobility can be improved by doping, which places additional charge carriers in the valence or conduction band. For inorganic semiconductors, atomic replacement of just a few parts per billion dopes these materials enough to become effective conductors. In contrast, the density of charge carriers needed to increase the conductivity of conjugated polymers by several orders of magnitude is quite high, and can be on the order of parts per thousand or even parts per hundred.[1–3]

Doping of plastic semiconductors is achieved by either oxidizing (for p-type doping) or reducing (for n-type doping) the conjugated polymer. The oxidation/reduction of conjugated polymers can be accomplished through a variety of means, including electrochemical doping,[4–6] which uses an applied bias and counterions from an electrolyte, or direct electrical methods, such as gate-doping in a field-effect transistor.[5,7] To permanently dope polymers, the best approach is chemical doping by adding a molecule to a conjugated polymer that is either a strong electron donor or acceptor, so that ground-state charge transfer reactions occur to produce equilibrium charge carriers.

Of course, conjugated polymers are full of defects (chain ends, oxidized or chemically altered monomers, kink sites, catalyst left over from the synthesis, *etc.*), that can trap or localize a charge carrier. Moreover, the low dielectric constant of organic semiconductors allows the carriers created by doping to have strong Coulomb interactions with the dopant counterions, interactions that are largely screened in doped inorganic materials. This means that at low doping concentrations in conjugated polymers, the carriers (also referred to as polarons) created are largely trapped. At higher concentrations, molecular doping is expected to create free carriers that contribute to improved charge transport and thus can be used as charge injection layers for organic–organic interfaces with good connections to organic active layers.[1] Applications of highly-doped semiconducting polymers include spintronics, thermoelectrics, and biological sensors as well as OLEDs and polymer-based solar cells.[8–12]

Much of the work studying conjugated polymer doping has focused on the prototypical semiconducting polymer, poly(3-hexylthiophene-2,5-diyl) (P3HT), whose chemical structure is pictured at the top left in Fig. 1.[1] One of the more common molecular dopants is 2,3,5,6-tetrafluoro-7,7,8,8-tetracyanoquinodimethane (F4TCNQ), whose chemical structure is shown in the upper right of Fig. 1. F4TCNQ has its LUMO level at 5.24 eV relative to vacuum, in a position, relative to the HOMO/valence band of P3HT at 5.2 eV,[13] to allow electrons to be transferred from P3HT to F4TCNQ, creating holes on P3HT.[2] F4TCNQ doping of P3HT dramatically increases the polymer's electrical conductivity by multiple orders of magnitude, although at the highest doping levels explored, the conductivity is observed to plateau with increased dopant loading.[3]

There are two main questions concerning the doping of polymers like P3HT with dopants like F4TCNQ that we will explore in this paper. First is the issue of

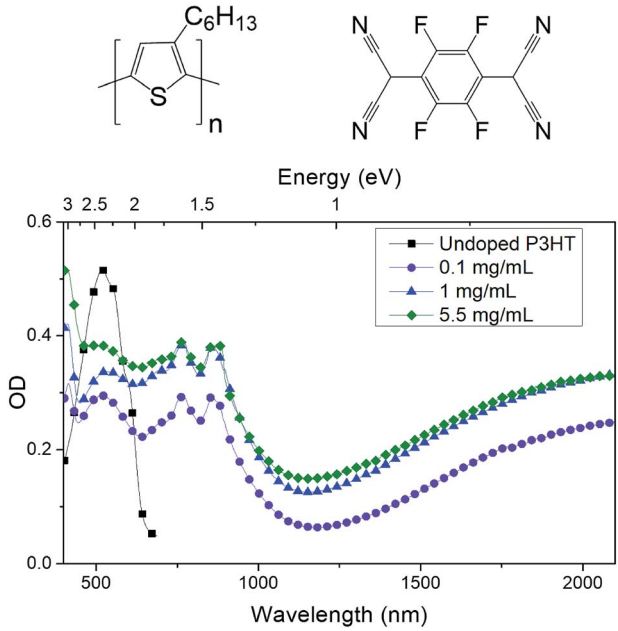

Fig. 1 Top Right: the chemical structure of the dopant F4TCNQ (2,3,5,6-tetrafluoro-7,7,8,8-tetracyanoquinodimethane). Top Left: the chemical structure of P3HT (poly(3-hexylthiophene-2,5-diyl). Lower Panel: steady-state UV-Vis-NIR absorption spectra of: an undoped P3HT film (black squares); an identical P3HT film after sequential doping using a 5.5 mg mL^{-1} solution of F4TCNQ in 70 : 30 THF : DCM (green diamonds); an identical P3HT film sequentially doped with a 1 mg mL^{-1} solution of F4TCNQ in DCM (blue triangles); and an identical P3HT film sequentially doped using a solution that was 0.1 mg mL^{-1} F4TCNQ in DCM (purple circles).

free *versus* trapped carriers in molecularly-doped conjugated polymer films. Previous work has estimated that ~95% of the polarons created by F4TCNQ-doping of P3HT at low concentrations remain trapped due to Coulomb binding with the F4TCNQ anion.[2] It is not clear, however, how this number changes with doping concentration or how Coulomb binding changes the spectroscopic and electrical properties of the polarons created by doping. Structural studies suggest that F4TCNQ resides in the lamellar region of P3HT crystallites, causing a reorganization of the P3HT crystal structure; F4TCNQ is also thought to increase order in the amorphous region of P3HT films.[14,15] Thus, the first main question we address in this paper is: can we use spectroscopic methods to separate the contributions of free and trapped carriers, and in doing so determine where the counterion resides relative to the polarons?

The second main issue we address in this work is the electronic nature of the charged carriers created by doping. The standard picture of doping for inorganic semiconductors, which has been extended to doped conjugated polymers, is shown in Fig. 2a and b.[16,17] The electronic structure associated with the polarons, however, can change if the holes pair at high concentrations to form bipolarons (Fig. 2c) or if the holes can delocalize to a neighboring P3HT chain as well as along the chain backbone (Fig. 2d).[18] Moreover, there are even competing theories as to the intrinsic electronic structure of a polaron, with a recent alternative model that

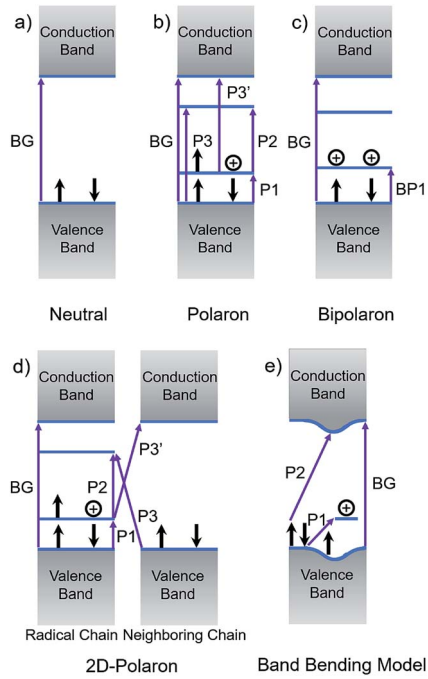

Fig. 2 (a) The band diagram for neutral semiconducting polymers, which shows only a single optical transition (labeled BG) and (b) the traditional, longstanding electronic structure model for polarons in semiconducting polymers and their corresponding optical transitions. The P3 and P3′ transitions are usually believed to be optically forbidden. (c) The traditional model for bipolarons and their allowed BP1 optical transition and (d) the model for 2-D-delocalized polarons, where optical transitions can occur both on the chain containing the majority of the radical cation character as well as diagonally between that chain and a neighboring, predominantly neutral chain. This makes the P3 and P3′ transitions become optically allowed and breaks their degeneracy. (e) A new band-bending model for the electronic structure of polarons on conjugated polymers that does not predict that a positively-charged polymer chain is easier to ionize than a neutral polymer chain.[19] There are no bipolarons or P3 or P3′ transitions in this model.

we refer to as the 'band-bending' model, which puts the polaronic states in the valence band rather than the bandgap, shown in Fig. 2e.[19–22] All of these different pictures predict different allowed transitions between the different polaronic electronic states. Thus, the second question we will address in this paper is: by studying the ultrafast relaxation dynamics of photoexcited polarons, can we distinguish between the various theoretical scenarios of polaron electronic structure outlined in Fig. 2?

To address both of these questions, we performed a series of ultrafast spectroscopy experiments examining the behavior of photoexcited polarons in F4TCNQ-doped P3HT films. We find clear evidence for two distinct polaron populations with different relaxation dynamics, which we assign to free and Coulombically-trapped polarons. By monitoring how the amplitudes of the two species change as the excitation wavelength is tuned, we are able to disentangle the spectra of the free and trapped polarons in our samples. We find that, perhaps counterintuitively, the number of trapped polarons increases with increasing

doping levels, with the trapped polaron spectrum blue-shifting at higher doping concentrations. We also find that based on the features of the transient spectroscopy, there is little evidence for bipolaron formation at high doping levels. Instead, the transient spectroscopy appears to be consistent with that expected for 2-D-delocalized polarons, and not with band-bending models in which the electronic states of hole polarons lie in the valence band rather than the bandgap. Taken together, our results help to build a better understanding of how polarons in doped conjugated polymers contribute to electrical conductivity.

2 Methods

2.1 Sample preparation

All of the F4TCNQ-doped P3HT films in this work were prepared *via* solution sequential processing[3] to ensure high optical quality and control over the doping levels. Briefly, 120 nm thick films of undoped P3HT (purchased commercially from Rieke Metals) were fabricated by spin-coating a 20 mg mL^{-1} solution of P3HT in *o*-dichlorobenzene at 1000 rpm for 60 s onto glass substrates. The films were then doped following the solution sequential processing procedure outlined by Scholes *et al.*[3] by spinning solutions of F4TCNQ on top of the pristine P3HT films at 4000 rpm for 10 s. For lower doping levels ($\leq$1 mg mL^{-1}), the F4TCNQ solutions were prepared in dichloromethane, which is known to swell but not dissolve P3HT, allowing for infiltration of the dopant into the P3HT underlayer. For higher doping levels of 5.5 mg mL^{-1}, the F4TCNQ dopant was dissolved in a 70 : 30 v/v tetrahydrofuran : dichloromethane mixture, with the THF fraction needed to solubilize the higher concentration of dopant. All samples were stored under an inert argon atmosphere at 1 atm and all measurements were taken with the samples in an inert atmosphere within 72 hours of fabrication to limit any effects from F4TCNQ subliming or other de-doping mechanisms that could affect the sample over time.

2.2 Transient absorption spectroscopy

All of the ultrafast transient absorption experiments were performed using a commercial Ti:sapphire regenerative amplifier (Coherent, Inc.) and a Helios transient absorption spectrometer that together provide $\sim$75 fs time resolution. The amplified laser system produced pulses of light at 800 nm with $\sim$3 mJ of energy at a 1 kHz repetition rate. Part of the amplified 800 nm beam was used to pump an optical parametric amplifier, which was used to create $\sim$10 μJ pulses at 1200, 1500, 1700, or 2000 nm to serve as the pump beam. The other part of the 800 nm pulse was focused into a sapphire plate to generate white light continuum in either the NIR (850 to 1300 nm) or visible regions (450 to 725 nm) to serve as the probe beam. We note that for both the NIR- and visible-probe experiments, scatter from the laser fundamental prevented transient absorption data from being collected in the region near 800 nm. The timing between the pump pulse and the probe pulse was modulated using a double-pass delay stage. Scans were averaged over at least 5 seconds per time point and at least three independent scans were taken.

2.3 Deconvoluting the transient absorption spectroscopy *via* differential kinetics

To determine the nature of the underlying and overlapping species in the ultrafast transient absorption measurements, we used the matrix decomposition technique Singular Value Decomposition. Singular Value Decomposition, which we applied according to methods elaborated by Doan *et al.*, factorizes a set of data into its significant components.[24] In our application, we took the data to be a function of wavelength on one dimension, and represented time steps, excitation wavelength and dopant concentration on the other dimension. Data was used from delays of 0.3 ps to 20 ps and for probe wavelengths from 500 to 720 nm and 900 to 1120 nm, including excitation of both 1 mg mL^{-1} and 5.5 mg mL^{-1} samples at 1200 nm, 1500 nm, 1700 nm and 2000 nm.

In our application of SVD, D holds the spectral components of our system, which is calculated from U, S, and V, which come from the Singular Value Decomposition of the data set in wavelength, excitation wavelength and concentration and time, along with F, which is a fitted model of how the measured absorption spectra change in time, excitation wavelength, and concentration:

$$\text{Data} = USV^{\mathrm{T}} = DF^{\mathrm{T}} \quad (1)$$

$$D = US(V^{\mathrm{T}}F^{\mathrm{T}+}) \quad (2)$$

We constructed the model F as a two-column matrix that described independent exponential decays for the two components. One row of F represents the fast component and the other the slow component. F is thus a function of the decay constants τ_1 and τ_2, which correspond to the fast and slow decay components, respectively, as well as the initial relative amplitudes of each component at each excitation wavelength and doping concentration. The columns of F run over time, describing the exponential decay of each component as a function of the initial amplitude of the spectral component and the time constant of its exponential decay.

We started by modeling the transient absorption data following 1200 nm excitation of the 1 mg mL^{-1} F4TCNQ-doped P3HT sample. After modeling this transient absorption decay, the matrix F would then be used to map out the decay following 1500 nm excitation, then that at 1700 nm excitation and so forth. This procedure was then repeated for the transient absorption data for different excitation wavelengths on the 5.5 mg mL^{-1} F4TCNQ-doped P3HT films. The two spectral components were constrained to have the same shape, regardless of excitation wavelength and doping concentration.

The difference between the transient absorption data and DF^{T} was minimized using a least squares technique to solve for the ratio of amplitudes, the spectral shape of the components, and the time constants of each component's exponential decay. Our attempts to include a third spectral component did not change the overall fit, as the first two components remained essentially unchanged and the third component had nearly zero amplitude.

Based upon initial fitting, the spectral shape and decay rate of each component were assumed to be constant for each excitation wavelength and the initial amplitude of each component was varied based upon the dopant concentration

and excitation wavelength. We also explored several other models, such as one component decaying into the other or an inverse time dependence for the decay of one component, but none of the alternative models fit the data better, and most of the other models had more fitting parameters than the simple model of two independently-decaying transient species.

Error bars were generated by fixing the ratio of the slow and fast components' starting amplitudes for the corresponding excitation wavelength, and calculating the root-mean-square error of the fit for a particular fitting parameter. The ratio of the root-mean-square error of the constrained fit to the unconstrained fit compared well to an estimate of the general variance of the data constructed by fitting four time-dependent single-probe-wavelength traces for each excitation wavelength and concentration to the simple model and averaging their root-mean-square errors.

3 Results and discussion

3.1 The electronic structure of polarons and bipolarons in conjugated polymer films

One of the key motivators for the experiments we present here is that the nature of the electronic quasiparticle species present in doped semiconducting polymers has been the subject of debate in the literature.[2,16,19,20,22,25] The basic band structure of a neutral conjugated polymer is shown in Fig. 2a. When the neutral polymer becomes positively doped, the polymer relaxes from a benzoid to a quinoid structure to stabilize the charge, creating a polaron.[16] In the standard picture, this rearrangement shifts the occupied half-filled state from the valence band into the bandgap and lowers an equivalent state from the bottom of the conduction band, leading to the situation in Fig. 2b.[16] Within this picture, doping should lead to three new optical transitions in addition to the original bandgap transition: the P1 transition, which consists of exciting an electron from the valence band to the half-filled state, the P2 transition, which involves exciting the electron in the half-filled state to the other state inside the bandgap, and a degenerate pair of transitions known as P3 and P3′, which involve excitation of an electron between the valence band and the empty state or between the half-filled state and the conduction band, respectively.[16]

For an ideal, doped single conjugated polymer chain, the P3 and P3′ transitions are optically forbidden, but in a disordered system or a material in which there is partial delocalization of the polarons between neighboring polymer chains (so-called 2-D delocalization), one or both of these transitions may be observable.[18,25] In this 2-D delocalization picture, shown in Fig. 2d, one polymer chain carries most of the radical cation character, but there can be optical transitions involving electrons to or from neighboring chains.[18] When this happens, the P3 and P3′ transitions become symmetry-allowed and the P2 transition is expected to become partially optically forbidden.[18] In addition, with 2-D-delocalization the P3 and P3′ transitions are no longer required to be degenerate in energy.

At high doping levels, it is possible that polarons on conjugated polymers can pair, forming bipolarons. This is because it can be energetically less costly to put two like charges near each other than to distort the backbone of the conjugated polymer in two separate locations.[16] Bipolaron formation is particularly likely

when the concentration of dopants is so high that the delocalization of polarons becomes limited by the total concentration of carriers.[16] Fig. 2c shows the standard electronic structure picture for bipolaron formation, in which there are two empty states within the bandgap, with the only optically-allowed transition going from the valence band to the lower-energy empty intragap state, termed the BP1 transition.[16,26,27]

Recently, however, several groups have proposed a new electronic structure scheme to explain polaron formation in doped conjugated polymers.[19,20] The new scheme, which is summarized in Fig. 2e, was motivated by the physical idea that it should be harder to ionize a positively-doped conjugated polymer chain than a neutral chain; the standard picture predicts that the half-filled polaronic state is closer to the vacuum level than the valence band.[19] In this new 'band-bending' model, which is based on density functional theory calculations, when a polaron forms, the state from which the electron was removed splits in half. After the state splits, a half-occupancy state containing the remaining electron bends below the bandgap into the valence band and the half-filled state containing the hole rises into the gap. The conduction band then bends down locally with the hole, forming another state that projects into the gap. The P1 transition would then result from promotion of an electron from the valence band to the intergap state and the P2 transition would arise when as valence band electron is promoted to the lowered part of the bent conduction band. Rather than being optically forbidden, there are no P3 or P3′ transitions in the band-bending model.[19,20] The band-bending model also provides no obvious mechanism for bipolaron formation.[19]

When a polaron is in close spatial proximity to its counteranion, the polaron can localize and become trapped in the Coulomb well of the counteranion.[2,28] Both experimental and theoretical work indicates that trapped polarons have a blue-shifted P1 peak due to their decreased delocalization and the presence of the Coulomb well.[23,29–31] Spano and his co-workers have pioneered calculations of polaron localization and trapping as a function of the distance of a counteranion from the doped polymer chain. These calculations show a clear shift to smaller wavelengths as well as a change in shape of the absorption band as the counteranion moves closer to the polaron, as shown in Fig. 3.[23] Of course, there may be an inhomogeneous distribution of free and weakly or more deeply trapped polarons in any given conjugated polymer film, but it is clear that polarons can absorb in different spectral regions depending on their degree of delocalization, which is directly related to their proximity to a dopant counterion.

Overall, there is still a great deal of complexity and controversy when it comes to describing polaronic states in conjugated polymers. There are multiple different pictures of the electronic structure of polarons, including the possibilities of traditional polarons, 2-D delocalized polarons and the new band-bending picture of polaron electronic structure. When this is combined with the fact that most polarons in chemically-doped conjugated polymer films are thought to be coulombically trapped rather than freely mobile, it is simply not at all clear how to best interpret the spectroscopy of doped conjugated polymer films. Our goal in this paper is to elucidate the spectroscopy of doped conjugated polymers by performing the ultrafast transient absorption experiments: as we will see below, the shape of

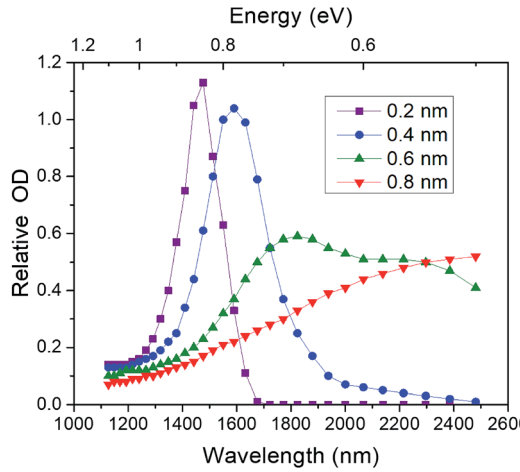

Fig. 3 A reproduction of theoretical calculations of the P3HT P1 polaron absorption band as a function of an anion distance from the P3HT chain, taken from ref. 23. As the anion distance decreases from 0.8 nm to 0.2 nm, the P1 peak shifts towards smaller wavelengths and narrows significantly.[23] The calculations used a 10-mer of P3HT with a point-charge counteranion situated at the given distance away from the center of the polymer chain, along with a dielectric constant and a Huang-Rhys parameter of 1.0.[23] The vibrational frequency was chosen to be 0.17 eV, the intrachain coupling to be −0.4 eV, the Gaussian disorder width to be 0.3 eV, and the homogeneous linewidth to be 0.03 eV.[23] See ref. 23 for details.

the excited-state absorption spectrum will tell us about polaron electronic structure, and the dynamics will tell us about the degree of coulombic polaron trapping.

3.2 The steady-state spectroscopy of F4TCNQ-doped P3HT films

We begin our study of the electronic structure of doped conjugated polymers in Fig. 1, which shows the steady-state optical absorption spectra of a neutral P3HT film (black squares) and P3HT films doped *via* sequential processing[3,32] with increasing concentrations of F4TCNQ (purple circles, blue triangles and green diamonds). The figure shows clearly that as neutral P3HT becomes doped, the absorption associated with the bandgap transition at 525 nm decreases in intensity, while new absorbing features grow in at 400, 700, 780, 880 and 2400 nm. All of these features have been observed in previous work and their assignments are well understood.[33–36] The peak near 2400 nm is assigned to the low-energy P1 transition of polarons on the doped P3HT. The new peaks that appear at 700, 780, and 880 nm are vibronic structure associated with the F4TCNQ anion, and the new peak at 400 nm is associated with neutral F4TCNQ.[33] We also expect that much of the absorption in the 650–900 nm region is the result of a P2 transition (and possibly P3 and/or P3′ transitions) that lie underneath the F4TCNQ anion absorption in this region.

Fig. 1 also shows that as the dopant concentration increases from 0.1 mg mL^{-1} to 1.0 mg mL^{-1}, the intensity of the doped P3HT P1 and P2/F4TCNQ anion absorption peaks increases. As the dopant concentration is further increased to 5.5 mg mL^{-1}, however, there is no further increase in the absorption intensity of

these peaks; instead, a shoulder appears on the high-energy side of the broad P1 band in the region between 1200 and 1500 nm. This new absorption feature could be consistent with that expected for the BP1 transition of bipolarons that form at high dopant concentrations,[16] but it also is potentially consistent with the P1 transition of single polarons that are coulombically localized by their counterions.[14]

3.3 Connection between the electronic structure and expected ultrafast dynamics of doped conjugated polymer films

To better understand the spectral changes that take place upon doping P3HT with different concentrations of F4TCNQ, we performed a series of pump/probe transient absorption experiments. Most groups have used three-pulse pump-probe experiments to study polarons, in which a first laser pulse is used to create a polaron, a second, time-delayed pulse excites the polaronic species, and then a third pulse probes the resulting spectral dynamics.[37–41] These experiments suffer from being unable to cleanly excite polarons with the second laser pulse because of spectral congestion from other excited-state species (excitons, triplets, *etc.*).[37,42–44] Here, we excite already-formed polarons in our F4TCNQ-doped P3HT films, avoiding spectral congestion. Our idea was to perform one set of experiments exciting the low-energy P1 peak near 2400 nm (0.5 eV), and a second set of experiments exciting at wavelengths further to the blue to learn more about the nature of the absorbing species that gives rise to the blue shoulder at higher doping concentrations.

Fig. 4 shows roughly what can be expected in our pump/probe experiments based on the traditional model for the electronic structure of polarons and bipolarons in conjugated polymers,[16] with time flowing from left to right. For the case of polarons, shown in the upper part of the figure, exciting the low-energy P1 transition should bleach both the P1 peak and the neutral bandgap absorption since an electron is removed from the valence band. The addition of a second electron in the intra-gap state should also lead to an increase in absorption of the P2 peak. In this picture, one can think of exciting the P1 band as taking an electron from the valence band and using to fill the pre-existing polaronic hole, leaving a new hole somewhere else in the material; in other words, the P1 transition is essentially a charge-transfer band for moving the hole polaron from one place in the polymer to another. Once the polymer backbone relaxes around the new hole, which should take place relatively quickly, the electronic states will rearrange to recover the initial electronic configuration and thus the equilibrium absorption spectrum.

If we extend these ideas to the case of 2-D-delocalized polarons, in addition to all of the aforementioned changes in absorption, we would expect that exciting the P1 band of the polaron would also bleach the now-allowed P3 transition and cause a corresponding increase in absorption intensity for the P3′ transition. If the P3 and P3′ transitions are degenerate, then there would be no net change in absorbance at the P3 transition energy, but if the degeneracy is broken, this could produce an additional transient absorption signature.

This picture could change even further in the case of trapped polarons, where the P1 transition will occur at a higher energy, and the positions of the P2, P3, and P3′ peaks all will shift depending on how Coulomb trapping affects the

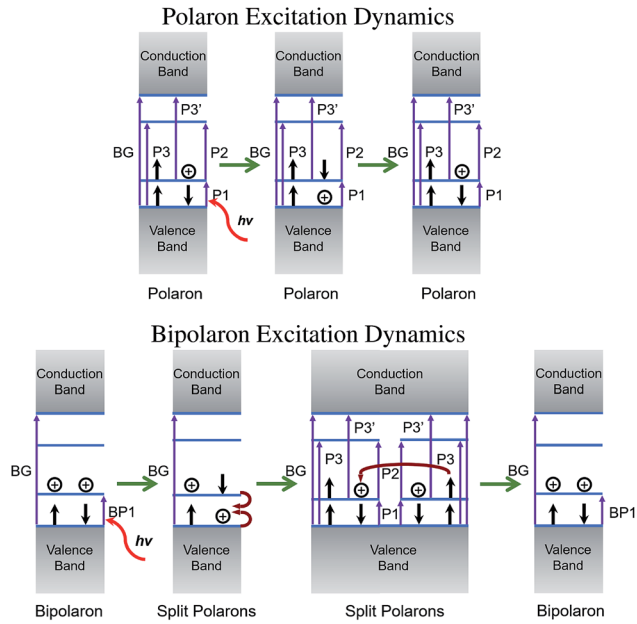

Fig. 4 Band diagrams explaining the dynamics expected following photoexcitation of polarons (top) and bipolarons (bottom) in the traditional conjugated polymer electronic structure picture; time flows from left to right. Following excitation of the low-energy polaron P1 transition, an electron is removed from the valence band and used to fill the pre-existing hole, creating a half-filled lower state and a filled P1 state. After rapid relaxation around the new hole, the system returns to the original ground-state polaron configuration. In contrast, when the BP1 transition of bipolarons is excited, an electron is taken from the valence band and used to fill one of the two holes, creating two single polarons in half-filled orbitals in different locations in the film. After any fast relaxation processes are complete, the two separated polarons must diffuse back together to reform the equilibrium bipolaron state, a process that is expected to occur on longer timescales.

corresponding energy levels. In the band-bending model of polaron electronic structure, the picture would be modified yet again, as exciting the P1 polaron band should temporarily bleach the P1, P2 and neutral bandgap transitions and there are no P3 or P3′ transitions to potentially bleach or increase in absorption intensity.

Finally, the lower part of Fig. 4 shows our expectations following excitation of the BP1 band of bipolarons. Here, one can think of the BP1 band as a charge-transfer transition that takes an electron from the valence band and moves it to fill one of the two original paired holes. This effectively dissociates the bipolaron into two single polarons, one of which remains in the original bipolaron location and the other of which appears somewhere else. Following excitation of the BP1 band, we expect both the BP1 and neutral bandgap transitions to be bleached by removal of the electron from the valence band. The two polaron-like states created will have new P1- and P2-like absorptions, and depending on the degree of delocalization between neighboring chains, there also could be new P3 and P3′ absorption transitions. As time progresses, the split single polarons will diffuse until they ultimately recombine back into an equilibrium bipolaron. Currently,

there are no predictions regarding how bipolaron states might be affected upon excitation for the band-bending model.[19,20]

3.4 Pump-probe transient absorption spectroscopy of F4TCNQ-doped P3HT

To understand the nature of the steady-state optical absorption spectrum of F4TCNQ-doped P3HT shown in Fig. 1, we started by performing pump/probe experiments exciting near the peak of the P1 transition. Fig. 5 shows that when exciting the 1 mg mL^{-1} F4TCNQ-doped P3HT film at 2000 nm, there is a bleach of the P3HT neutral bandgap transition at 525 nm (2.4 eV), a second bleach that appears near 650 nm (1.9 eV), and a new, broad transient absorption that appears near 1000 nm (1.24 eV). The transient bleaches and absorption all decay at similar rates, suggesting that they all arise from the same electronic species.

These transient spectral signatures are not consistent with what is expected from the traditional polaron model outlined at the top of Fig. 4. In this picture, we would expect bleaching of the bandgap transition at 525 nm and an increase in absorption of the P2 transition near 1000 nm, but there is no way to explain the bleach that appears near 650 nm, below the bandgap of neutral P3HT. Instead, the data in Fig. 5 are consistent with the photoexcitation of 2-D delocalized polarons, with the 1000 nm transient absorption corresponding to the expected increase in the P2 transition and the 650 nm bleach corresponding to removal of the partially-allowed P3 transition. We might also expect 2-D delocalized polarons to show an increase in absorption due to the P3′ transition, but this is likely obscured by scatter from the laser fundamental at 800 nm (or possibly has significant overlap with the P3 and/or P2 bands). It is also worth noting that the bleach of the P3 transition at 650 nm is not consistent either with the

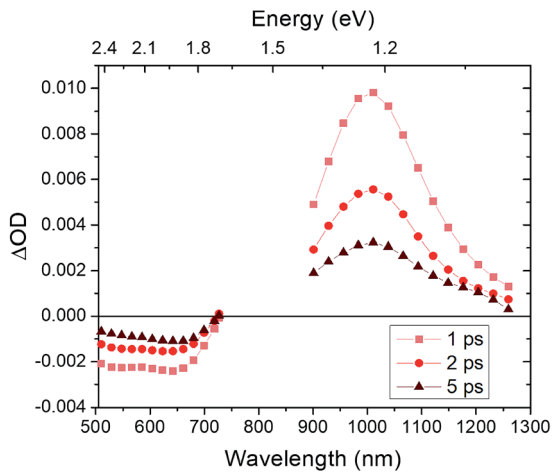

Fig. 5 Ultrafast transient absorption spectra of P3HT films sequentially doped with a 1 mg mL^{-1} F4TCNQ solution in DCM following excitation at 2000 nm; spectra are shown at delays of 1, 2, and 5 ps between excitation and collection. The data show two bleaches in the visible region, at 520 nm and 650 nm, and one broad transient absorption in the visible region near 1000 nm, which we assign to the bleach of neutral P3HT, the bleach of the P3 transition, and an increase of the P2 transition in the 2-D-delocalized polaron picture, respectively (*cf.* Fig. 2d).

photoexcitation of bipolarons, which would show increased absorption at this wavelength, or with the band-bending model, which does not predict any P3 or P3′ transitions.[19,20]

With the basic features of the ultrafast transient spectroscopy of polarons on P3HT established, we turn next to identifying the nature of the species that contributes to blue shoulder of the P1 band seen for P3HT at higher doping concentrations in Fig. 1. To this end, we repeated the experiment using a series of different excitation wavelengths spanning the range from 1200 to 2000 nm; the results for three such wavelengths are shown in Fig. 6. As we tune the excitation wavelength to the blue, we see clear shifts in the P2 transient absorption of P3HT that peaks near 1000 nm. In particular, the higher the energy of the excitation wavelength, the more blue-shifted the peak of the resulting P2 transient absorption. Moreover, higher-energy excitation also leads to a broadening on the blue side of the P2 transient absorption signature. But most importantly, the data in Fig. 6 show that transient absorption no longer decays uniformly with time: the blue side of the transient absorption that is enhanced when exciting further to the blue decays more slowly than the peak of the transient absorption band. All of these observations indicate that bluer excitation wavelengths are indeed accessing a new electronic species that was not significantly excited at 2000 nm.

To better understand the origin of the new electronic species, we also repeated our ultrafast transient absorption experiments on P3HT films as a function of dopant concentration. Fig. 7 shows the results when the bluest wavelength, 1200 nm, is used to excite P3HT films sequentially doped with F4TCNQ at concentrations of 1 mg mL^{-1} (red-colored curves) and 5.5 mg mL^{-1} (blue-colored curves). The data show that as the doping concentration is increased, the transient absorption spectrum shifts to the blue and shows a broadening on the blue

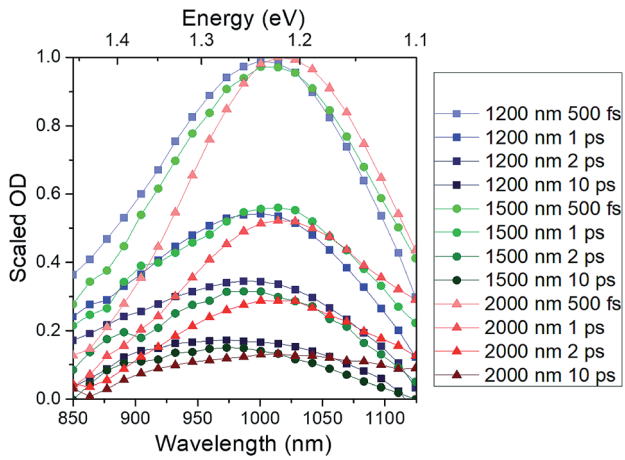

Fig. 6 Ultrafast transient absorption spectra of a P3HT film sequentially doped with a 1 mg mL^{-1} F4TCNQ solution in DCM following excitation at either 1200 nm (blue squares), 1500 nm (green circles) or 2000 nm (red triangles). Data are shown at 0.5, 1, 2, and 10 ps delays between excitation and collection, with darker colors used for later delay times. The observed transient absorption feature shifts to the blue, with the blue feature decaying more slowly, as the excitation wavelength is tuned to the blue.

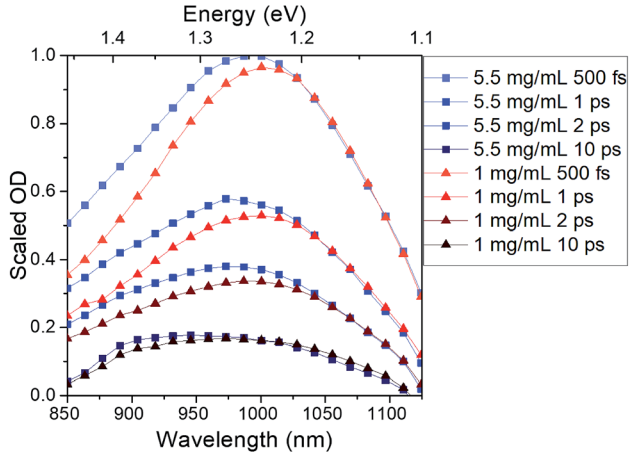

Fig. 7 Ultrafast transient absorption spectra of P3HT films that have been sequentially doped either with a 1 mg mL^{-1} solution of F4TCNQ in DCM (red triangles) or a 5.5 mg mL^{-1} solution of F4TCNQ in a 70 : 30 v/v mixture of THF : DCM (blue squares) following excitation at 1200 nm. Data are shown for 0.5, 1, 2, and 10 ps delays between excitation and collection, with darker colors corresponding to later delay times. The more highly-doped samples have the transient absorption shifted to the blue and the blue feature decaying more slowly than the lower-doped sample.

side, similar to what is seen when using higher-energy excitation. Moreover, also like what we saw above, the blue portion of the transient absorption spectrum decays more slowly than the peak. Thus, whatever the new electronic species is, its presence is manifest both when exciting at higher energies and when the doping concentration is increased.

3.5 Analysis of the ultrafast transient absorption spectra of F4TCNQ-doped P3HT films

To elucidate the nature of the second electronic species that is excited more at 1200 nm than 2000 nm and is more prevalent in P3HT films doped with F4TCNQ at 5.5 mg mL^{-1} than at 1 mg mL^{-1} doping level, we globally analyzed our transient absorption data across excitation wavelength and doping concentration. For our global analysis, we assumed a model in which there are precisely two species excited in the doped films. Each species in the model has a different absorbance at each excitation wavelength, is present in different amounts at different doping concentrations, and each has its own transient absorption spectrum and decay rate. We then used SVD, as described above, to extract the transient absorption spectra and decay times of each of the two species.

With the SVD procedure applied globally to all of our transient absorption data for the 1 and 5.5 mg mL^{-1}-doped samples (not just the subset of data shown in Fig. 5–7), we found that indeed SVD yielded a quickly-decaying (lifetime of ~0.37 ps), red-shifted transient absorption component with a larger initial amplitude and a more slowly-decaying (lifetime of ~15 ps), blue-shifted transient absorption component with a lower initial amplitude. The spectra of the two components are shown in Fig. 8. Based on their shapes, it makes sense to assign both of the

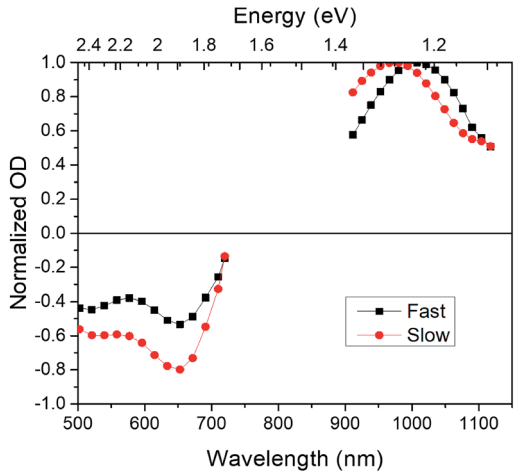

Fig. 8 The two spectral components extracted using SVD from our global fits to the transient absorption spectra of P3HT films sequentially doped with several different concentration solutions of F4TCNQ and excited at multiple wavelengths. The more slowly-decaying component (red circles) has a ~15 ps lifetime while the faster decaying component (black squares) has a 0.37 ps lifetime. Both components have two clear negative peaks in the visible region, at 530 nm and 650 nm, corresponding to bleaches of the BG and P3′ transitions. The slow component, which we assign to trapped polarons, shows a blue-shifted P2 peak in the NIR and more intense bleaching in the visible region relative to that of the fast component, which we assign to free polarons.

spectral components as arising from what would be expected following photo-excitation of a 2-D-delocalized polaron, with a bleach of the bandgap and P3 transitions and the transient appearance of P2 and P3′ peaks. Our hypothesis is thus that the two species can be assigned to free and coulombically-trapped 2-D-delocalized polarons: the species with the redder transient absorption spectrum and faster decay corresponds to that from free polarons, while the species with the blue-shifted transient absorption spectrum and slower recovery corresponds to trapped polarons.

To better characterize the SVD components, we fit each of the two SVD components that describe the transient spectroscopy to a sum of four Gaussian peaks, with the idea that each Gaussian peak reflects one of the expected transient 2-D-delocalized polaron transitions. Both the slow- and the fast-decaying spectral components, which we assign to trapped and free polarons, have two negative Gaussian peaks in the visible region, corresponding to the bleaches of bandgap and P3 transitions. Both transient spectra also have two positive Gaussian peaks, corresponding to newly-created P3′ and P2 absorptions. The Gaussian fitting parameters for both transient species are summarized in Table 1.

The Gaussian fits to the two SVD spectral components summarized in Table 1 make sense in terms our assignment of these as transitions arising from excited 2-D-delocalized polarons. As seen in Fig. 2d, the energy of the P2 transition plus twice the energy of the P1 transition should equal the optical bandgap energy, as should the sum of P3 and P3′ transition energies minus the P2 transition energy. In both cases, the energies of the fitted Gaussian peaks sum to within ~0.1 eV of the known ~2.2 eV bandgap of P3HT.[45]

Table 1 Fitted Gaussian peak locations for the free and trapped polaron spectral components

Assignment	Wavelength (nm)	Energy (eV)	Amplitude	Width (eV)
Free polarons				
Neutral	517	2.40	−0.45	0.22
P3′	658	1.89	−0.52	0.16
P3	765	1.62	0.12	0.17
P2	1000	1.24	1	0.11
P1	2400	0.52	N/A	N/A
Trapped polarons				
Neutral	519	2.39	−0.60	0.22
P3′	670	1.85	−0.86	0.19
P3	742	1.67	0.48	0.12
P2	969	1.28	1	0.11
P1	1500	0.83	N/A	N/A

With this assignment of the two transient species as arising from free and trapped polarons, the ∼0.37 and ∼15 ps time constants we observe imply that photoexcited free polarons in P3HT recover roughly forty times faster than the trapped polarons. This makes sense given what we expect from the standard 2-D-delocalized polaron picture. For free polarons, photoexcitation relocalizes the polaron and the system recovers to equilibrium as soon as the polymer backbone can relax to accommodate the hole in its new location, a process that can easily happen on sub-ps time scales. For coulombically-trapped polarons, it is reasonable to expect that the excited-state absorption is slightly blue-shifted from that of free polarons, much like the ground-state absorption spectra of free and trapped polarons shown above in Fig. 3. Moreover, we expect that photoexcitation of coulombically-bound polarons likely moves the hole away from the trap site, to where it must diffuse back to recover to equilibrium. Since diffusion is a much slower process (and since we expect polarons near traps to have lower mobilities than their free counterparts), it is not surprising that the excited-state recovery of trapped polarons is more than an order of magnitude slower than that of free polarons.

We turn next to exploring the relative amplitudes of the free and trapped polaron transient absorptions at each excitation wavelength and both doping levels. Fig. 9 shows the ratio of the slow (trapped) to fast (free) polaron components as a function of excitation wavelength for the 5.5 mg mL^{-1}-doped sample (upper panel) and the 1 mg mL^{-1}-doped sample (lower panel). The figure makes clear that more of the slow transient absorption component is excited near 1400 nm than at other wavelengths, particularly in the 5.5 mg mL^{-1}-doped sample. This fits perfectly with our expectation that trapped polarons absorb to the blue of free polarons, and that the blue shoulder observed on the P1 band of the 5.5 mg mL^{-1}-doped sample (Fig. 1) is indeed due to the presence of an increased number of trapped polarons. The fact that many of the polarons added at high doping concentrations are trapped fits well with the observation that doping at this level does not improve the overall film conductivity.[3,14]

Given our assignment of the two transient absorption species to free and trapped 2-D-delocalized polarons, one important question that needs to be

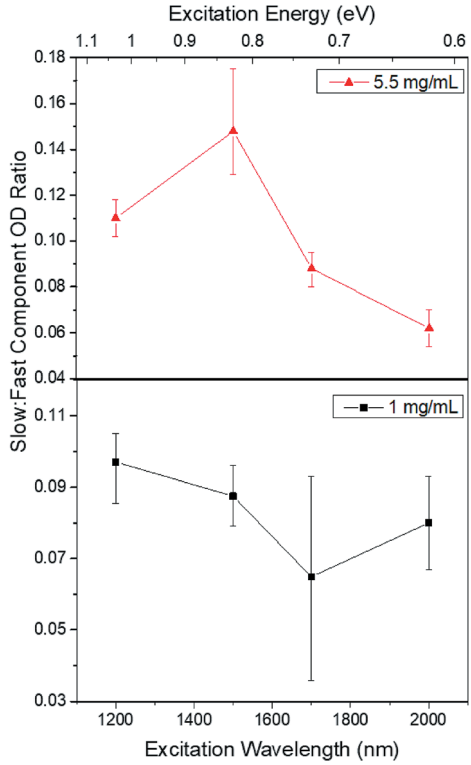

Fig. 9 The ratio of the initial optical densities of the extracted slow to fast components from the global fit of the transient absorption measurements as a function of excitation wavelength for: (a) a P3HT film sequentially doped with a 5.5 mg mL^{-1} F4TCNQ solution, and (b) a P3HT film sequentially doped with a 1 mg mL^{-1} F4TCNQ solution. It is clear that there is more of the slow component produced using 1200 and 1500 nm excitation wavelengths, particularly for the more highly-doped sample.

addressed is why does the number of trapped polarons appear to increase at higher doping concentrations? Previous work has shown that when P3HT is doped by F4TCNQ at low concentrations, the dopant intercalates into the lamellar regions of the P3HT crystallites, leading to a reorientation of the P3HT crystalline unit cell.[14,46–48] Because the F4TCNQ anion sits in the lamellar region, it lies relatively far from the P3HT backbone where the polaron resides, thus minimizing the Coulomb interaction between them. Once the crystalline reorganization is complete, there is no room for additional dopant in the P3HT crystallites, so at high doping concentrations F4TCNQ is forced to reside in the amorphous regions of the P3HT films. We speculate that when the anion is in the amorphous regions of the film, it can sit closer to the polymer backbone, thus increasing the Coulomb attraction and the degree of polaron trapping.

We also can analyze the relative amplitudes of free and trapped polarons in Fig. 9 in another way. If we follow the logic in the preceding paragraph, we can assume that the 0.1 mg mL^{-1}-doped P3HT sample has a negligible amount of trapped polarons. This means that the P1 band of this film is largely that of free polarons. If we then scale our measured ratio of trapped-to-free polarons by the

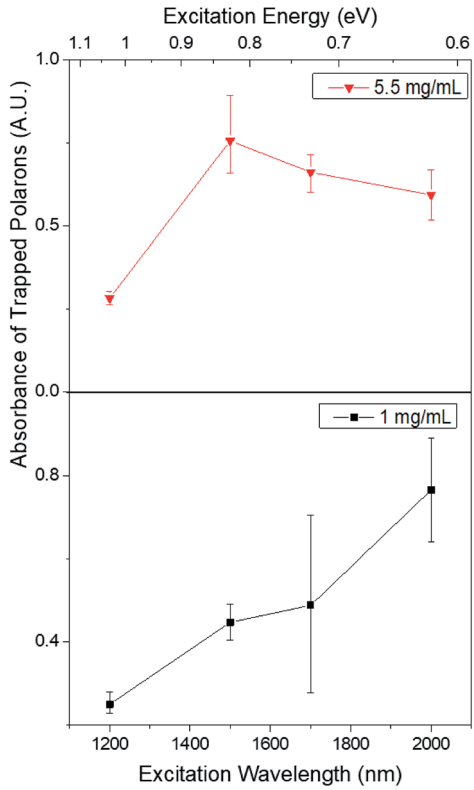

Fig. 10 The calculated action spectrum of trapped polarons for: (a) a P3HT film sequentially doped with a 5.5 mg mL^{-1} F4TCNQ solution, and (b) a P3HT film sequentially doped with a 1 mg mL^{-1} F4TCNQ solution. This spectrum was calculated by scaling the measured ratios of the slow to fast components in Fig. 9 by the absorption of a P3HT films sequentially doped with a 0.1 mg mL^{-1} F4TCNQ solution, which we expect has few trapped polarons. The data make clear that the more highly-doped sample has trapped polarons with a more blue-shifted absorption spectrum, indicating that these polarons are more highly trapped than those in the lower-doped sample.

0.1 mg mL^{-1}-doped film absorption spectrum, we can obtain the absorption spectrum of the trapped polarons in the higher-doped P3HT films. These spectra, which are one of the principal results of this work, are shown in Fig. 10. Essentially, these are reconstructed action spectra of the slow transient absorption component that we assign to the presence of trapped polarons.

The data in Fig. 10 make clear that the spectrum of trapped polarons is different at different doping concentrations. If we compare our extracted trapped polaron action spectra to what is expected from theory (Fig. 3, above),[14,23,29] we can estimate the average distance the polaron lies from its counterion at each doping concentration. We accomplished this by using a least squares regression to fit our measured action spectra of the trapped polaron in P3HT films doped with different F4TCNQ concentrations to a weighted sum of the simulated polaron spectra for varying anion distances,[23] as shown in Fig. 11. We conclude that the 'free' polarons in 0.1 mg mL^{-1}-F4TCNQ-doped P3HT films are still somewhat coulombically bound by their counterions, with an average polaron-to-anion

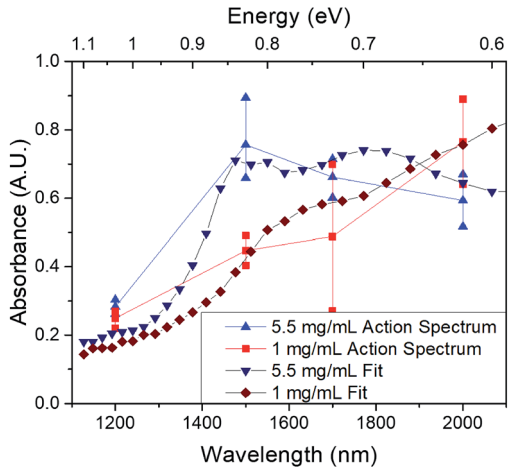

Fig. 11 The action spectra of trapped polarons from Fig. 10 fit to linear combinations of the anion-distance-dependent P1 spectra calculated by Spano and co-workers shown in Fig. 3.[23] The 5.5 mg mL^{-1} F4TCNQ-doped P3HT film (blue triangles) fits best to a sum of the theoretical spectra with anion distances calculated for 0.2, 0.4, and 0.6 nm spacing between the anion and the polymer chain with 20, 7, and 73% relative weightings, respectively. The 1 mg mL^{-1} F4TCNQ-doped P3HT film (red squares) fits best to a sum of the spectra for anion distances calculated for 0.4, 0.6, and 0.8 nm spacing between the anion and the polymer chain with 6, 4 and 90% relative weightings, respectively.

distance of 0.7 to 0.9 nm, consistent with the idea that the dopant counterions sit in the lamellar regions of the P3HT crystallites. We also see that the distance between the trapped polarons in the 5.5 mg mL^{-1}-doped P3HT films and their F4TCNQ counteranions is 0.2 nm to 0.6 nm, and the corresponding distance in the 1 mg mL^{-1}-doped films is 0.4 to 0.8 nm. This also fits well with our idea that at increased dopant concentrations, the dopant sits in the amorphous region of the film where it can reside closer, on average, to the polarons on the P3HT backbone.

As a check on the validity of our assignments of the peaks observed in the transient spectroscopy, we worked to reconstruct the 0.1 mg mL^{-1} UV-Vis spectrum (Fig. 1), which should result almost entirely from free polarons, by using the fitted peak positions and widths of the fast transient spectral component (Table 1), along with the known spectra of neutral P3HT and anionic F4TCNQ. The results, which also make use of a single Gaussian to represent the P1 absorption band, are shown in Fig. 12. Clearly, our ability to fit the steady-state UV-Visible absorption spectrum with only amplitudes as adjustable parameters is excellent. This lends credence to the idea that there are indeed 2-D-delocalized P3, P3′ and P2 transitions lying under the sharp F4TCNQ anion peaks in the UV-Vis of doped P3HT.

Finally, we are also able to check our understanding of the various polaronic transitions by working to reproduce the steady-state absorption spectrum of the 5.5 mg mL^{-1}-F4TCNQ-doped P3HT sample using the trapped polaron action spectrum extracted from our ultrafast spectroscopic analysis. Here, we started with the 0.1 mg mL^{-1}-doped-P3HT steady-state spectrum, and added additional absorption from the action spectrum for trapped polarons that we extracted from the slow transient absorption component. Fig. 13 shows that again, the results are

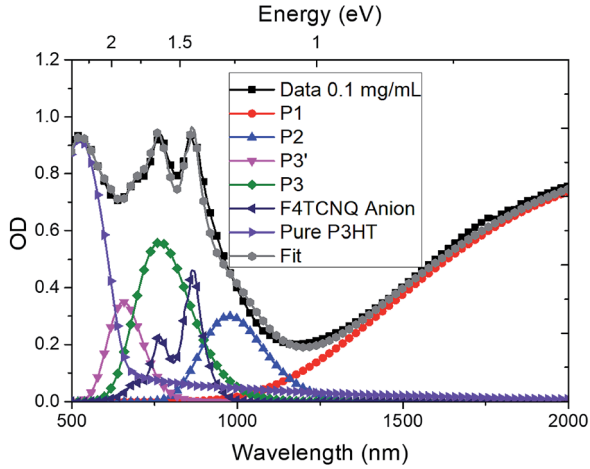

Fig. 12 Reconstruction of the absorption spectrum of a P3HT film sequentially doped with a 0.1 mg mL^{-1} solution of F4TCNQ in DCM using a linear combination of the known F4TCNQ anion spectra (taken from Wang *et al.*),[33] the known spectrum of neutral P3HT (Fig. 1), and the Gaussian fits of the peak positions of the fast component (which we assign to free polarons) extracted from the global model of our transient absorption measurements (Table 1); see text for details. The excellent agreement between the measured spectrum and the reconstructed fit shows that our transient absorption measurements, global fit, and steady-state absorption measurements are all internally consistent.

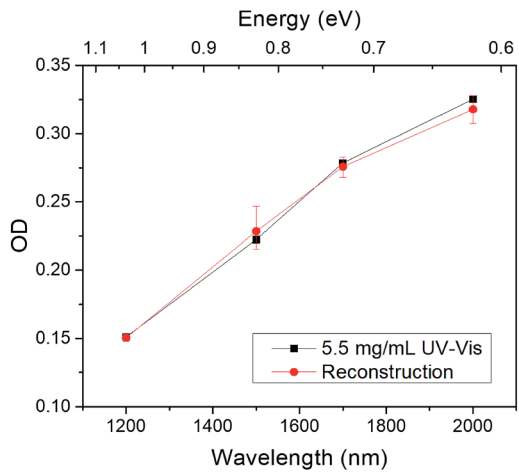

Fig. 13 Reconstruction of the absorption spectrum of a highly-doped P3HT film (created using a 5.5 mg mL^{-1} solution of F4TCNQ). The reconstructed spectrum uses the spectrum of a low-doped P3HT film (created using an 0.1 mg mL^{-1} F4TCNQ solution) and the action spectrum of trapped polarons that we extracted from the ultrafast transient absorption data in Fig. 10; see text for details. The excellent agreement provides confirmation that the action spectrum taken from our ultrafast measurements can be used to account for the spectral shape changes observed between the high- and low-doped P3HT films seen in Fig. 1.

excellent. Thus, the spectra of trapped polarons that we extracted from our ultrafast spectroscopy experiments are indeed internally-consistent with the measured steady-state spectra at each doping level.

4 Conclusions

In this paper we have found strong evidence for two populations of quasiparticles present in F4TCNQ-doped P3HT. The transient spectroscopy is consistent with F4TCNQ-doped P3HT consisting primarily of free and trapped polarons, both of which follow the traditional model for 2-D-delocalized polarons in terms of their observed absorption transitions. Neither the band-bending picture of polarons nor the presence of bipolarons accounts for the observed bleaches in our transient absorption measurements. We were able to distinguish free and trapped polarons by monitoring both the position and dynamics of their transient spectra: trapped polarons show blue-shifted features that decay more than an order of magnitude more slowly than free polarons, a direct result of their need to diffuse to return to equilibrium and their generally poor mobility.

By monitoring the relative amounts of free and trapped polarons produced at different excitation wavelengths, we were able to generate an action spectrum to disentangle the steady-state absorption of the two polaronic species. We found that the more highly-doped samples had greater amounts of polarons that were more tightly bound by their counterions. By comparing the action spectra of trapped polarons to theory, we found that the F4TCNQ dopant resides roughly 0.4 nm away from trapped polarons, compared to 0.7 to 0.9 nm for free polarons. For an F4TCNQ anion to be that close to a trapped polaron, it likely must pi-stack with the P3HT backbone, presumably in the amorphous regions of the film.

With an internally-consistent view of the electronic structure of free and trapped polarons in place, it may now be possible to design new materials to improve carrier mobility by decreasing the fraction of trapped polarons. For example, the use of dopants whose anions are electrostatically shielded from their corresponding holes provides a possible route to preventing the build-up of trapped polarons at high doping levels.[49,50] Another possibility would be to engineer the crystal structure of a polymer to better accommodate counterions into the lattice in positions far from the backbone, so that more dopants can be accommodated without having to produce significant numbers of trapped polarons. The hope is that with our new understanding, it should be possible to create new materials that do not suffer from increased polaron trapping at high doping concentrations.

Conflicts of interest

There are no conflicts of interest to declare.

Acknowledgements

This work was supported by the National Science Foundation under grant numbers CBET-1510353 and CHE-1608957. This material is based upon work supported by the National Science Foundation Graduate Research Fellowship under Grant No. DGE-1650604. Any opinion, findings, and conclusions or

recommendations expressed in this material are those of the authors and do not necessarily reflect the views of the National Science Foundation.

References

1 F. Deschler, D. Riedel, A. Deák, B. Ecker, E. V. Hauff and E. Da, *Synth. Met.*, 2015, **199**, 381–387.
2 P. Pingel and D. Neher, *Phys. Rev. B: Condens. Matter Mater. Phys.*, 2013, **87**, 115209.
3 D. T. Scholes, S. A. Hawks, P. Y. Yee, H. Wu, J. R. Lindemuth, S. H. Tolbert and B. J. Schwartz, *J. Phys. Chem. Lett.*, 2015, **6**, 4786–4793.
4 C. Francis, D. Fazzi, S. B. Grimm, F. Paulus, S. Beck, S. Hillebrandt, A. Pucci and J. Zaumseil, *J. Mater. Chem. C*, 2017, **5**, 6176–6184.
5 E. Lim, K. A. Peterson, G. M. Su and M. L. Chabinyc, *Chem. Mater.*, 2018, **30**, 998–1010.
6 C. Enengl, S. Enengl, S. Pluczyk, M. Havlicek, M. Lapkowski, H. Neugebauer and E. Ehrenfreund, *ChemPhysChem*, 2016, **56**, 607–622.
7 J. Yamamoto and Y. Furukawa, *Org. Electron.*, 2016, **28**, 82–87.
8 M. Cox, E. H. M. van der Heijden, P. Janssen and B. Koopmans, *Phys. Rev. B: Condens. Matter Mater. Phys.*, 2014, **89**, 085201.
9 S. Y. Yang, B. N. Kim, A. A. Zakhidov, P. G. Taylor, J. K. Lee, C. K. Ober, M. Lindau and G. G. Malliaras, *Adv. Mater.*, 2011, **23**, 184–188.
10 G. Lu, J. Blakesley, S. Himmelberger, P. Pingel, J. Frisch, I. Lieberwirth, I. Salzmann, M. Oehzelt, R. Di Pietro, A. Salleo, N. Koch and D. Neher, *Nat. Commun.*, 2013, **4**, 1588.
11 P. Bujak, I. Kulszewicz-Bajer, M. Zagorska, V. Maurel, I. Wielgus and A. Pron, *Chem. Soc. Rev.*, 2013, **42**, 8895.
12 L. Sudha Devi, M. K. Al-Suti, C. Dosche, M. S. Khan, R. H. Friend and A. Köhler, *Phys. Rev. B: Condens. Matter Mater. Phys.*, 2008, **78**, 1–8.
13 P. P. Khlyabich, B. Burkhart and B. C. Thompson, *J. Am. Chem. Soc.*, 2011, **133**, 14534–14537.
14 D. T. Scholes, P. Y. Yee, J. R. Lindemuth, H. Kang, J. Onorato, R. Ghosh, C. K. Luscombe, F. C. Spano, S. H. Tolbert and B. J. Schwartz, *Adv. Funct. Mater.*, 2017, **27**, 1702654.
15 A. Hamidi-Sakr, L. Biniek, S. Fall and M. Brinkmann, *Adv. Funct. Mater.*, 2016, **26**, 408–420.
16 J. L. Bredas and G. B. Street, *Acc. Chem. Res.*, 1985, **18**, 309–315.
17 M. Nowak, S. D. D. V. Rughooputh, S. Hotta and A. J. Heeger, *Macromolecules*, 1987, **20**, 965–968.
18 D. Beljonne, J. Cornil, H. Sirringhaus, P. J. Brown, M. Shkunov, R. H. Friend and J.-L. Brédas, *Adv. Funct. Mater.*, 2001, **11**, 229–234.
19 G. Heimel, *ACS Cent. Sci.*, 2016, **2**, 309–315.
20 R.-Q. Png, M. C. Ang, M.-H. Teo, K.-K. Choo, C. G. Tang, D. Belaineh, L.-L. Chua and P. K. Ho, *Nat. Commun.*, 2016, **7**, 11948.
21 K. Kohlstedt, *ACS Cent. Sci.*, 2016, **2**, 278–280.
22 S. Kahmann, D. Fazzi, G. J. Matt, W. Thiel, M. A. Loi and C. J. Brabec, *J. Phys. Chem. Lett.*, 2016, **7**, 4438–4444.
23 R. Ghosh, A. R. Chew, J. Onorato, V. Pakhnyuk, C. K. Luscombe, A. Salleo and F. C. Spano, *J. Phys. Chem. C*, 2018, **122**, 18048–18060.

24 S. C. Doan and B. J. Schwartz, *J. Phys. Chem. C*, 2013, **117**, 4216–4221.
25 J. Cornil and J.-L. Brédas, *Adv. Mater.*, 1995, **7**, 295–297.
26 Y. H. Kim, S. Hotta and A. J. Heeger, *Phys. Rev. B: Condens. Matter Mater. Phys.*, 1987, **36**, 7486–7490.
27 K. E. Ziemelis, A. T. Hussain, D. D. C. Bradley and R. H. Friend, *Phys. Rev. Lett.*, 1991, **66**, 2231–2234.
28 V. I. Arkhipov, E. V. Emelianova, P. Heremans and H. Bässler, *Phys. Rev. B: Condens. Matter Mater. Phys.*, 2005, **72**, 235202.
29 A. R. Chew, R. Ghosh, Z. Shang, F. C. Spano and A. Salleo, *J. Phys. Chem. Lett.*, 2017, **8**, 4974–4980.
30 M. J. Bird, J. Bakalis, S. Asaoka, H. Sirringhaus and J. R. Miller, *J. Phys. Chem. C*, 2017, **121**, 15597–15609.
31 S. Kahmann, M. A. Loi and C. J. Brabec, *J. Mater. Chem. C*, 2018, **18**, 10270–10280.
32 I. E. Jacobs, E. W. Aasen, J. L. Oliveira, T. N. Fonseca, J. D. Roehling, J. Li, G. Zhang, M. P. Augustine, M. Mascal and A. J. Moulé, *J. Mater. Chem. C*, 2016, **4**, 3454–3466.
33 C. Wang, D. T. Duong, K. Vandewal, J. Rivnay and A. Salleo, *Phys. Rev. B: Condens. Matter Mater. Phys.*, 2015, **91**, 085205.
34 J. Gao, B. W. Stein, A. K. Thomas, J. A. Garcia, J. Yang, M. L. Kirk and J. K. Grey, *J. Phys. Chem. C*, 2015, **119**, 16396–16402.
35 F. M. McFarland, C. M. Ellis and S. Guo, *J. Phys. Chem. C*, 2017, **121**, 4740–4746.
36 J. Fuzell, I. E. Jacobs, S. Ackling, T. F. Harrelson, D. M. Huang, D. Larsen and A. J. Moulé, *J. Phys. Chem. Lett.*, 2016, **7**, 4297–4303.
37 O. G. Reid, R. D. Pensack, Y. Song, G. D. Scholes and G. Rumbles, *Chem. Mater.*, 2014, **26**, 561–575.
38 E. Lioudakis, I. Alexandrou and A. Othonos, *Nanoscale Res. Lett.*, 2009, **4**, 1475–1480.
39 A. Saeki, S. Seki, Y. Koizumi and S. Tagawa, *J. Photochem. Photobiol., A*, 2007, **186**, 158–165.
40 H. Li, A. Gauthier-Houle, P. Grégoire, E. Vella, C. Silva-Acuña and E. R. Bittner, *Chem. Phys.*, 2016, **481**, 281–286.
41 F. Provencher, N. Bérubé, A. W. Parker, G. M. Greetham, M. Towrie, C. Hellmann, M. Côté, N. Stingelin, C. Silva and S. C. Hayes, *Nat. Commun.*, 2014, **5**, 4288.
42 M. Menšík, J. Pfleger and P. Toman, *Chem. Phys. Lett.*, 2017, **677**, 87–91.
43 S. Das, P. P. Khlyabich, B. Burkhart, S. T. Roberts, E. Couderc, B. C. Thompson and S. E. Bradforth, *J. Phys. Chem. C*, 2014, **118**, 6650–6660.
44 H. Ohkita, S. Cook, Y. Astuti, W. Duffy, S. Tierney, W. Zhang, M. Heeney, I. McCulloch, J. Nelson, D. D. C. Bradley and J. R. Durrant, *J. Am. Chem. Soc.*, 2008, **130**, 3030–3042.
45 A. Guerrero, S. Loser, G. Garcia-Belmonte, C. J. Bruns, J. Smith, H. Miyauchi, S. I. Stupp, J. Bisquert and T. J. Marks, *Phys. Chem. Chem. Phys.*, 2013, **15**, 16456–16462.
46 A. Hamidi-Sakr, L. Biniek, J.-l. Bantignies, D. Maurin, L. Herrmann, N. Leclerc, P. Lévêque, V. Vijayakumar and N. Zimmermann, *Adv. Funct. Mater.*, 2017, **1700173**, 1–13.
47 D. T. Duong, C. Wang, E. Antono, M. F. Toney and A. Salleo, *Org. Electron.*, 2013, **14**, 1330–1336.

48 J. Hynynen, D. Kiefer, L. Yu, R. Kroon, R. Munir, A. Amassian, M. Kemerink and C. Müller, *Macromolecules*, 2017, **50**, 8140–8148.
49 Z. Liang, Y. Zhang, M. Souri, X. Luo, A. M. Boehm, R. Li, Y. Zhang, T. Wang, D.-Y. Kim, J. Mei, S. R. Marder and K. R. Graham, *J. Mater. Chem. A*, 2018, **6**, 16495–16505.
50 T. J. Aubry, J. C. Axtell, V. M. Basile, K. J. Winchell, J. R. Lindemuth, T. M. Porter, J.-Y. Liu, A. N. Alexandrova, C. P. Kubiak, S. H. Tolbert, A. M. Spokoyny and B. J. Schwartz, *Adv. Mater.*, 2019, **31**, 1805647.

